Contents lists available at ScienceDirect

Journal of Crystal Growth

journal homepage: www.elsevier.com/locate/jcrysgro

# Growth and characterization of AlInN/GaN superlattices

Haotian Xue *, Elia Palmese, Ben J. Sekely, Brian D. Little, Fred A. Kish, John F. Muth, Jonathan J. Wierer *

*Department of Electrical and Computer Engineering, North Carolina State University, Raleigh, NC 27695, USA*

ARTICLE INFO

Communicated by Hongping Zhao

ABSTRACT

Data are presented on near-lattice-matched $Al_{1-x}In_xN$/GaN superlattices (SLs) with superior morphology to thick AlInN layers. The SLs are grown by metalorganic chemical vapor deposition and consist of ~ 3 nm thick AlInN, ~1 nm thick GaN layers, and $x = 0.153$ to 0.203. The SLs are grown with either 20 or 100 periods on GaN-on-sapphire or free-standing GaN substrates. Growth conditions are explored, and the In-content of the AlInN layers within the SL increases with growth temperature and pressure, while the growth rate decreases with pressure. Thick AlInN layers grown on GaN-on-sapphire exhibit island growth with a root mean square (rms) roughness of ~ 0.65 nm, while the AlInN/GaN SLs have steplike morphology and rms ~ 0.3 nm. Also, 80 nm thick AlInN/GaN SLs grown on GaN substrates exhibit nearly perfect steplike morphology with a lower rms of ~ 0.13 nm and extremely low pit densities. The refractive index of the SLs is the weighted average of AlInN and GaN, and they emit light from the quantum states within the thin GaN layers. These AlInN/GaN SLs are a potential replacement for AlInN layers in optoelectronic and electronic devices that require steplike morphology and controlled pitting.

## 1. Introduction

III-nitride (AlInGaN) semiconductors have had wide success in optoelectronic and electronic devices. Of the ternary alloys, AlInN is the least explored and implemented in devices. AlInN is useful because — it has a lattice-matched condition to GaN with a wider bandgap [1]; it provides a high refractive index contrast to GaN, which is useful for waveguiding or distributed Bragg reflectors [2–4]; its high polarization fields are used for barrier layers to create 2-dimensional electron gases in high-electron-mobility transistors (HEMTs) [5]; it has higher critical electric fields that can be used for power devices [6,7]; and it can be oxidized to create insulating layers for devices [8–10].

However, AlInN is difficult to implement in devices because of growth limitations that lead to poor morphology and pitting. The morphology of nearly-lattice matched AlInN layers greater than 50 nm thick suffers even with the best-known growth conditions. Island growth dominates, and the surface morphology consists of mounding on the surface that decorates the steplike surface of the underlying GaN [11,12]. Island growth is caused by low adatom surface mobility at lower growth temperatures [13]. AlInN layers with less In (not lattice matched to GaN) tend to be smoother but are strained [14], which limits their thickness. Also, pits that start from dislocations in the substrate or within the AlInN grow larger as the layer thickness increases [15]. Usually, thicknesses of AlInN are limited to ~ 200–300 nm before the surface becomes too rough or pitted, requiring thicker layers of GaN to be grown to recover the morphology, which limits its usefulness in devices.

Bulk layers of the other ternary alloys of AlGaN and InGaN also have limitations on thickness and composition due to lattice strain when grown on GaN [16,17]. It has been shown that SLs of AlGaN/GaN and InGaN/GaN with short periods (<10 nm) can be a method to ensure excellent surface morphology and prevent defects such as cracking, surface roughening, phase separation, dislocations, and pits that are formed due to lattice strain. In the case of AlGaN/GaN SL on GaN, it is a well-known method of strain management to prevent cracks [18] and suppress the generation of misfit dislocations [19]. These AlGaN/GaN SL have found practical uses in devices such as electron-blocking layers in light-emitting diodes (LEDs) [20], enhanced Mg doping [21], barriers in HEMTs [22–24], and cladding layers in laser diodes [25,26]. In the case of InGaN/GaN SLs on GaN, it is a method to avoid the critical thickness of InGaN that causes roughening and phase separation [27]. InGaN/GaN SLs are substitutes for thick InGaN layers in solar cells [28,29], and underlayers in LEDs [30].

There are fewer reports of AlInN/GaN SLs. It has been demonstrated as an underlayer in LEDs to prevent defects in the InGaN/GaN active layers [31], and to examine the incorporation of Indium in thin AlInN

* Corresponding authors.
*E-mail addresses:* hxue8@ncsu.edu (H. Xue), jjwierer@ncsu.edu (J.J. Wierer).

https://doi.org/10.1016/j.jcrysgro.2024.127567
Received 12 December 2023; Received in revised form 30 December 2023; Accepted 1 January 2024

layers grown at low pressures [32]. However, the surface morphology and the impact on pits compared to bulk AlInN layers has yet to be demonstrated.

This paper presents data on the growth and characterization of AlInN/GaN SLs. Growth parameters such as pressure, temperature, and substrate type are explored. The In-content of the AlInN layers within the SL increases with growth temperature and pressure, while the growth rate decreases with pressure. The AlInN/GaN SLs suppress the island growth present in bulk AlInN layers, and their surface exhibits superior morphology with lower roughness. SLs grown on GaN substrates have step-like morphology and extremely low pit densities. The SLs have a refractive index that is the weighted average of AlInN and GaN, and they emit light from the quantum states within the thin GaN layers.

## 2. Experimental methods

The samples are grown by metal–organic chemical vapor deposition (MOCVD) in a Taiyo Nippon Sanso Co. (TNSC) SR2328KS reactor. The layers are grown on commercially available free-standing GaN and GaN-on-sapphire substrates. The *c*-plane GaN substrates are single-side polished, ~450 μm thick, have an etch pit density of $< 5 \times 10^4$ cm$^{-2}$, n-type carrier concentration of $10^{19}$ cm$^{-3}$, and offcut ~ 0.3° towards the *m*-direction. The GaN-on-sapphire substrates are single-side polished, c-plane patterned sapphire and GaN layers with thicknesses of ~ 4.5 μm, etch pit density in the order of $10^8$ cm$^{-2}$, and n-type carrier concentration of $5 \times 10^{18}$ cm$^{-3}$.

The growth starts with a 350 nm thick and unintentionally doped GaN layer grown at 1150 °C and atmospheric pressure. For the SL samples, it is followed by 20 or 100 pairs of ~ 3 nm thick AlInN and ~ 1 nm thick GaN layers (total thicknesses of 80 nm or 400 nm) at varying temperatures and pressures. The thicknesses are chosen to prevent defects from forming and achieve an SL structure that is predominately formed from AlInN to retain its desirable properties (such as bandgap and refractive index). A 3 nm thick AlInN layer remains relatively smooth to avoid island growth and pitting, while the 1 nm thick GaN "repairs" the surface before the next AlInN layer is grown. The number of periods is chosen to be comparable with bulk AlInN layers demonstrated in the literature. Samples with 20 periods represent a thinner layer to compare to the surface morphology of AlInN, which remains relatively smooth. Samples with 100 periods represent a thicker layer where significant surface defects for AlInN are formed. The SLs are capped with a 2 nm thick GaN layer resulting from growth termination procedures. For comparison, thick (bulk) layers of AlInN that are either 80 nm or 400 nm thick are grown to match the SL thicknesses. All layers are grown in an $N_2$ ambient with a V/III ratio of ~ $1.44 \times 10^4$, and are unintentionally doped. The AlInN layers are grown with 10.6 μmol/min of TMAl and 9.5 μmol/min of TMIn, while the GaN layers are grown with 20 μmol/min of TEGa. The growth temperature and pressure are constant for all layers to avoid temperature or pressure ramping and growth interruptions.

Four sets of samples are grown for this study. The first set investigates the surface morphology and crystalline quality of the SLs compared to bulk AlInN layers of similar thickness. The second and third sets are AlInN/GaN SLs grown at different temperatures and pressures to study their effects, respectively. For the second set, the growth pressure for the SL varies from 10 kPa to 50 kPa in 10 kPa intervals, with the growth temperature kept constant at 775 °C. The growth time is adjusted to compensate for the change in growth rate related to pressure. In the third set, the growth temperature is varied between 775° to 800 °C with the pressure fixed at 30 kPa, resulting in 5 samples with indium content in the AlInN layers of 0.203, 0.192, 0.184, 0.166, and 0.153. The final set of AlInN/GaN SLs are grown on free-standing GaN substrates to compare with layers grown on GaN-on-sapphire templates. All the growth conditions for the samples described in this paper are shown in Table 1.

The near-lattice condition of $Al_{1-x}In_xN$ is determined by the equation:

$$a(GaN) = a(Al_{1-x}In_xN) = (1-x)\cdot a(AlN) + x\cdot a(InN) \quad (1)$$

where $x$ is the In content, $a(GaN)$ is the a-lattice (in-plane) constant of GaN, $a(AlN)$ is the a-lattice constant of AlN, and $a(Al_{1-x}In_xN)$ is the a-lattice constant of AlInN. The lattice constants of the binary alloys are $a(AlN) = 3.113$Å and $a(InN) = 3.538$Å. For GaN, the a-lattice constant can vary depending on the substrate where it is 3.189Å for GaN grown on c-plane sapphire and 3.183Å for GaN substrates [14]. The lattice-matched condition is $x \approx 0.17$, and higher and lower $x$ represent nearly lattice matched conditions.

The samples are characterized to determine structural and optical properties as follows. X-ray diffraction (XRD) ω-2θ scans of the (0002) reflection using a Philips XPert Pro is performed to determine the alloy fractions and layer thicknesses. Fitting the XRD data with the PANalytical Epitaxy and Smoothfit software packages determines the detailed layer structure. Scanning transmission electron microscopy (STEM) and energy-dispersive X-ray spectroscopy (EDS) are performed with a Thermo Fisher Titan 80–300 on cross sectioned samples by a focus ion beam (FIB) etching to observe the layers and interfaces. Surface morphology, pit density, and root mean square (rms) surface roughness are measured using a Digital Instruments Dimension 3100 atomic force microscope (AFM) with a standard tapping mode probe

**Table 1**
Growth parameters and characteristic results for all samples.

| | | Growth conditions | | | | XRD | AFM | | | |
|---|---|---|---|---|---|---|---|---|---|---|
| ID | Shown in Figs | Substrate | # of Periods | Press (kPa) | Temp (°C) | In (%) | RMS overall (nm) | RMS no pits (nm) | Pit den (×10$^7$cm$^{-2}$) | Pit Area (%) |
| M287 | 4(a) | GaN/$Al_2O_3$ | 100 | 20 | 775 | 18.1 | 1.675 | 0.843 | N/A | N/A |
| M289 | 2(a) | GaN/$Al_2O_3$ | 20 | 20 | 775 | 17.6 | 0.351 | 0.235 | 32.8 | 0.79 % |
| M300 | 4(a) | GaN/$Al_2O_3$ | 100 | 20 | 780 | 19.2 | 4.200 | 1.229 | N/A | N/A |
| M304 | 2(b), 3(a) | GaN/$Al_2O_3$ | 20 | 30 | 775 | 20.3 | 0.420 | 0.321 | 13.6 | 0.30 % |
| M308 | 2(c) | GaN/$Al_2O_3$ | 20 | 40 | 775 | 19.8 | 0.435 | 0.228 | 31.2 | 0.82 % |
| M309 | 2(e) | GaN/$Al_2O_3$ | 20 | 50 | 775 | 19.8 | 3.132 | N/A | N/A | N/A |
| M312 | 1(a), 3(d), 4(b) | GaN/$Al_2O_3$ | 20 | 30 | 790 | 16.6 | 0.364 | 0.299 | 13.6 | 0.24 % |
| M316 | 3(e) | GaN/$Al_2O_3$ | 20 | 30 | 800 | 15.3 | 0.317 | 0.226 | 12.4 | 0.23 % |
| M317 | 1(d), 4(a), (b) | GaN/$Al_2O_3$ | 100 | 30 | 790 | 17.2 | 1.449 | 0.613 | 9.2 | 1.23 % |
| M323 | 1(b) | GaN/$Al_2O_3$ | Bulk | 30 | 790 | 15.8 | 0.646 | N/A | N/A | N/A |
| M327 | 2(d) | GaN/$Al_2O_3$ | 20 | 10 | 775 | 17.5 | 1.880 | N/A | N/A | N/A |
| M332 | 1(c) | GaN/$Al_2O_3$ | Bulk | 30 | 790 | 17.6 | 0.470 | 0.390 | 33.2 | 0.64 % |
| M333 | 3(b) | GaN/$Al_2O_3$ | 20 | 30 | 784.5 | 19.2 | 0.602 | 0.437 | 29.6 | 0.35 % |
| M334 | 1(e) | GaN/$Al_2O_3$ | Bulk | 30 | 790 | 17.8 | 19.53 | N/A | N/A | N/A |
| M335 | 5(a), 6(a-c) | GaN | 20 | 30 | 790 | 19.5 | 0.202 | 0.162 | 2.8 | 0.07 % |
| M350 | 3(c) | GaN/$Al_2O_3$ | 20 | 30 | 787.5 | 18.4 | 0.560 | 0.397 | 33.2 | 0.35 % |
| M365 | 5(b), (c) | GaN | 20 | 30 | 815 | 13.7 | 0.132 | N/A | N/A | N/A |

with a tip radius of ~ 10 nm. The samples are measured optically using a J. A. Woollam V-Vase M−2000 spectroscopic ellipsometry (SE) and fit with CompleteEASE software to determine the refractive index [9,10]. Finally, cathodoluminescence (CL) is employed to determine emission properties of the SLs using a Horiba Scientific H-CLUE Spectroscopy and Imaging CL System attached to a JEOL 7600F SEM with a Gatan Alto Cryogenic Stage.

## 3. Results and discussion

Fig. 1(a) to (e) show the AFM of five samples grown to compare the surface morphology of bulk films and superlattices grown on GaN-on-sapphire substrates. Fig. 1(a) shows the surface of a 20-period (80 nm thick) $Al_{1-x}In_xN$/GaN SL ($x = 0.166$). It shows a very smooth surface (rms = 0.30 nm) with atomic steps closely resembling the underlying GaN layers. Pits caused by threading dislocations are present with a density of ~ $1.36 \times 10^8$ $cm^{-2}$ (obtained by counting pits in the AFM images), comparable to the dislocation density of the GaN-on-sapphire substrates before growth. Fig. 1(b) shows the surface of an 80 nm thick, bulk $Al_{1-x}In_xN$ ($x = 0.158$) layer with the same growth conditions as the SL shown in Fig. 1(a). It shows typical island growth (mounds) on AlInN surfaces aligning to the atomic edges of the underlying GaN with an rms of ~ 0.65 nm, comparable to AlInN layers reported in literature [12]. Another sample is grown to study the effect of a 3 nm GaN capping layer on top of an 80 nm thick bulk AlInN layer, shown in Fig. 1(c), to observe the recovery of surface morphology. Some surface morphology improvement stems from the GaN cap layer, but the typical mounds from the AlInN layer are still visible. This demonstrates that thinner layers of AlInN interspersed with thin GaN layers are required to keep the morphology intact. The capping layer better highlights the pits, and an increased number can be observed with a density of $3.3 \times 10^8$ $cm^{-2}$. The larger pit density of bulk AlInN layers compared to the SL shows how the SL suppresses the formation of pits.

Another pair of samples are grown to investigate the growth of significantly thicker AlInN/GaN SLs and bulk layers. Fig. 1(d) and (e) show a 100-period $Al_{1-x}In_xN$/GaN SL ($x = 0.172$) and a bulk $Al_{1-x}In_xN$ ($x = 0.178$) layer with the same ~ 400 nm total thickness, respectively. It is apparent that the SL exhibits superior surface morphology, with an rms of 0.61 nm compared to 19.53 nm for the bulk layer.

The effect of growth pressure on the AlInN/GaN SL morphology and In content is explored and shown in Fig. 2. The SLs grown at pressures of 20 kPa, 30 kPa, and 40 kPa exhibit good surface morphology (Fig. 2(b)-(d)), while at 10 kPa and 50 kPa, the surfaces roughen (Fig. 2 (d) and (e)). At 50 kPa, there are In inclusions on the surface. The rms roughness of the 20, 30, and 40 kPa samples are 0.235 nm, 0.321 nm, and 0.228 nm, respectively. Fig. 2(f) shows the dependence of growth rate and In-content of the AlInN layers with pressure. A decrease in the growth rate with increasing pressure is observed. This reduction is likely due to more pronounced pre-reactions. Therefore, the growth time per period is adjusted to achieve samples with the same approximate layer thicknesses. There is an increase in the In incorporation at the lowest pressures that plateaus at 30 kPa and possibly caused by more pronounced TMAl consumption due to pre-reactions [33], and increased In incorporation with higher growth pressure [34]. The best rms roughness is obtained with samples grown between 20 kPa and 40 kPa, and as a result, the rest of the samples presented in this study are grown at 30 kPa.

Fig. 3 shows 20-period AlInN/GaN SLs grown at 30 kPa and varying temperatures from 775 °C to 800 °C, resulting in 5 samples with indium content in the AlInN layers of 0.203, 0.192, 0.184, 0.166, and 0.153. Fig. 3(f) shows the indium content follows a downward trend with increasing temperatures, the same behavior as in bulk AlInN layers [35,36]. However, as seen in Fig. 3(a) to (e), the surface morphology does not suffer as significantly as bulk AlInN layers with increasing indium content [14], where typically the increase in In-content of AlInN leads to more pitting and surface roughening. All the SLs shown in Fig. 3 have step-like surfaces, and the pit densities do not show a significant trend with varying growth temperatures.

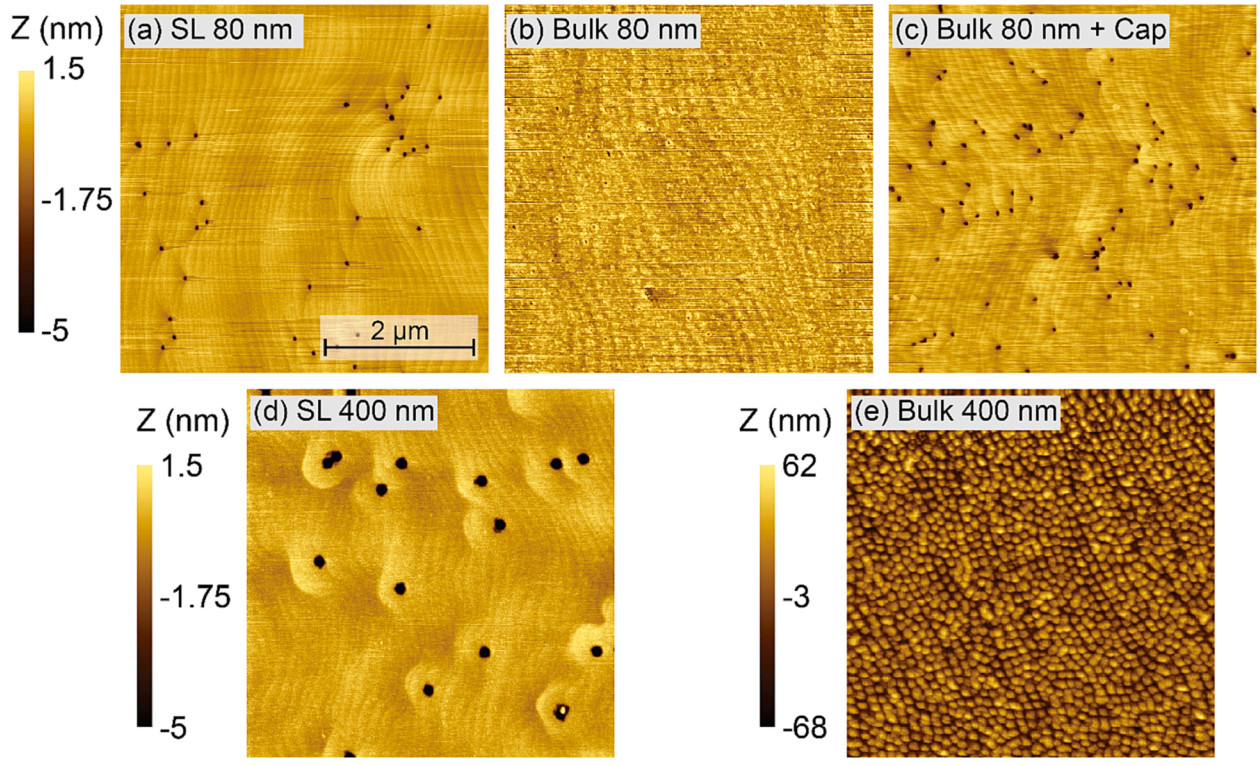


**Fig. 1.** Atomic force microscope (AFM) images of (a) 20 periods of 3 nm thick AlInN and 1 nm thick GaN superlattice (SL) with a 2 nm GaN capping layer, (b) 80 nm thick AlInN, (c) bulk AlInN with a 3 nm thick GaN capping layer, (d) 100 periods of 3 nm thick AlInN and 1 nm thick GaN superlattice with a 2 nm GaN capping layer, and (e) 400 nm thick AlInN. The SLs have significantly better surface morphology than bulk layers.

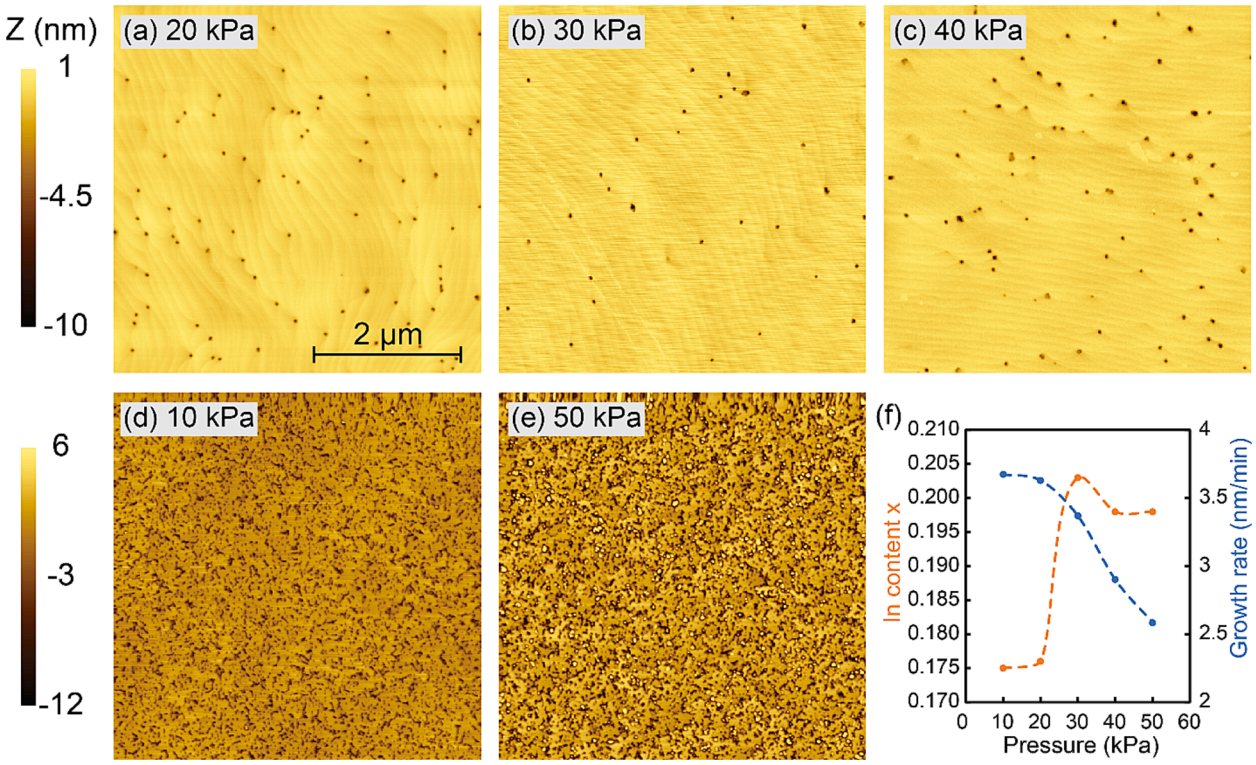


**Fig. 2.** Atomic force microscope (AFM) images of AlInN/GaN SLs grown at (a) 20 kPa, (b) 30 kPa, (c) 40 kPa, (d) 10 kPa, and (e) 50 kPa. The surfaces are smoothest between 20 and 40 kPa. Plot of (f) the In content, x, in the $Al_{1-x}In_xN$ and growth rate versus pressure. The x increases between 10 kPa and 30 kPa and plateaus after 30 kPa, and the growth rate shows a downward trend with higher growth pressure.

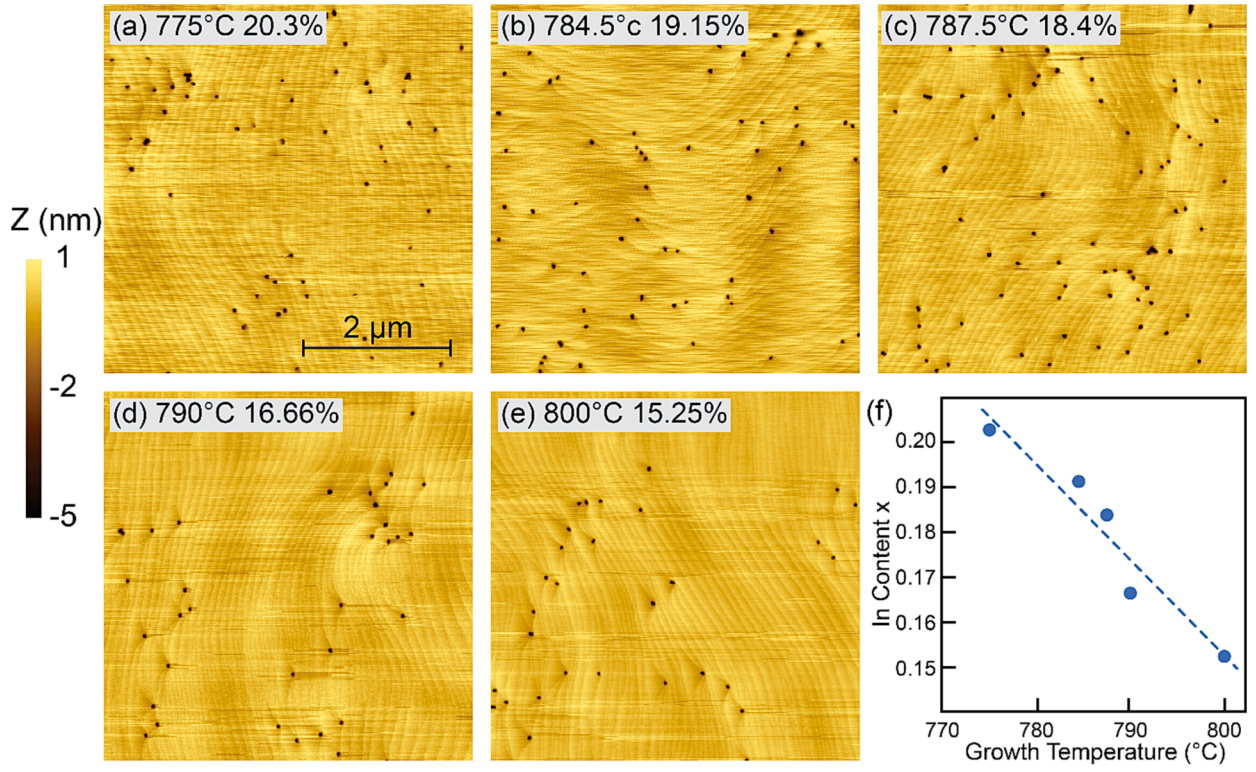


**Fig. 3.** Atomic force microscope (AFM) images of AlInN/GaN SLs with 20 periods that are grown at different temperatures, producing samples with In content, x, of (a) 0.203, (b) 0.192, (c) 0.184, (d) 0.166, and (e) 0.153. Plot of (f) AlInN In content x versus growth temperature.

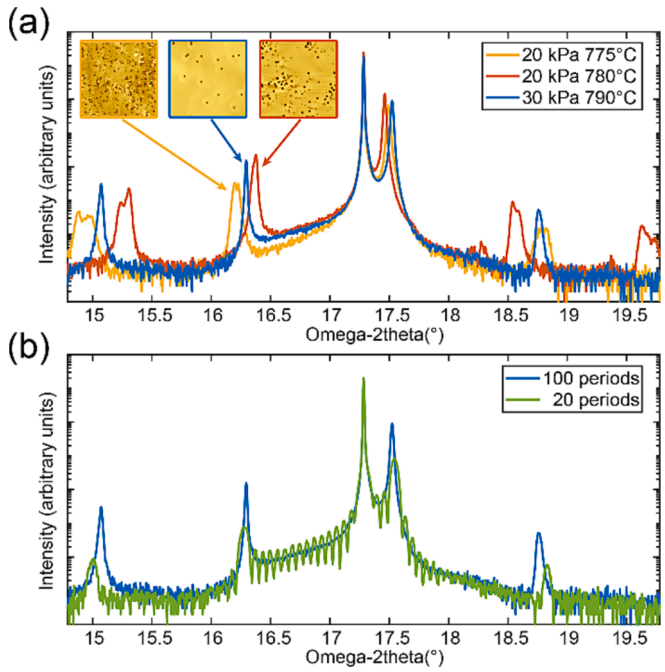


**Fig. 4.** (a) X-ray diffraction (XRD) ω-2θ scans in the (0002) direction of three AlInN/GaN SL samples. The three SLs are grown at pressures and temperatures of 20 kPa/775 °C, 20 kPa/780 °C, and 30 kPa/790 °C. The upper left insets show AFMs of the three samples, where 30 kPa and 790 °C are chosen as optimal with the best morphology. The XRD for this sample shows sharp single peaks, while the other two show double SL peaks and surfaces covered in pits. (b) XRD scan of two SLs with a different number of periods. The 20-period SL has SL peaks and fringe peaks to a high order, indicating good crystal quality and periodicity. The 100-period sample shows sharp SL peaks but no fringe peaks due to exceeding the XRD instrument resolution.

Fig. 4(a) shows the XRD omega-2-theta scans of three 400-nm-thick $Al_{1-x}In_xN$/GaN SLs grown with different conditions. It shows that the sample grown at our chosen optimal condition (30 kPa, 790 °C, $x = 0.172$) has narrow superlattice peaks, indicating a consistent layered structure throughout the 100 periods. As for the samples grown with suboptimal conditions (20 kPa, 775 °C, $x = 0.181$ and 20 kPa, 780 °C, $x = 0.176$), two sets of superlattice peaks are present, indicating the presence of two different period thicknesses within the SLs. The AFM image in the insets shows degraded surface morphologies for the sample with double superlattice peaks. A possible cause for peak doubling is a change in growth rate related to lattice relaxation and higher In content. Therefore, with thicker layers, the AlInN must be lattice matched with GaN. Fig. 4(b) compares the XRD scans of a 20-period and a 100-period SL. The 20-period SL has prominent superlattice and smaller fringe peaks, indicating good crystal quality. The 100-period SL has more intense superlattice peaks but no fringe peaks due to the number of periods that exceed the XRD resolution.

AlInN/GaN SLs are grown on free-standing GaN substrates to observe how surface morphology changes with In-content. They consist of 20 periods and are grown at 790 °C and 815 °C, with In contents of 0.195 and 0.137, respectively. An excellent surface with clearly visible atomic steps is observed for the 790 °C sample shown in Fig. 5(a). It has a surface roughness rms of 0.16 nm and pit density of $\sim 1.2 \times 10^7$ cm$^{-2}$. Fig. 5(b) and (c) show the AFMs for the SL grown at 815 °C with less indium. The surface morphology is even better, with a rms of 0.13 nm and nearly perfect step-like morphology. The angle offset from c-plane can be found by counting the number of steps in Fig. 5(b), combined with the AFM scan length of 5 μm and the c-lattice constant of GaN (5.185 Å). This yields an angle of 0.35°, close to the GaN substrate offcut. Pits are only observed in the larger area 20 μm × 20 μm scans and are most likely formed from the pits in the underlying GaN substrate ($<5 \times 10^4$ cm$^{-2}$). This quality level for surface morphology and pit density is not possible with AlInN bulk layers. Comparing these two samples, more pits form in the SL with higher indium content and tuning the In-content to control the pit density on GaN substrates is essential. The increase in pits with In-content is consistent with the behavior of AlInN bulk layers [36].

STEM is performed on the sample shown in Fig. 5(a), and the results are shown in Fig. 6. A highly periodic and consistent composition superlattice can be observed. The layer thicknesses match those determined from XRD. Due to the low pit density of the GaN substrates, no pits were observed across the entire FIB cross-section (~7 μm). A zoomed-in image is shown in Fig. 6(b), and an EDS line scan for the atomic fractions of Al, Ga, and In is shown in Fig. 6(c). There is noticeable intermixing between the GaN and AlInN layers, with small amounts of Al and In in the GaN layers and Ga in the AlInN layers. It is possible that the intermixing is caused by traditional layer disordering during growth [37], auto-incorporation of Ga from the surrounding chamber surfaces [38], and the FIB cross-sectioning. These periodically changing quaternary layers with less abrupt heterointerfaces may help improve electrical conductivity without sacrificing optical properties. Measuring electrical properties for these promising SLs is reserved for future work.

The refractive index of AlInN/GaN SL (Fig. 1(a)) is measured by Spectral Ellipsometry (SE) to compare to bulk layer AlInN (Fig. 1(b)) and GaN, and is shown in Fig. 7(a). The refractive index versus wavelength of the AlInN/GaN SL shows a weighted value between those of AlInN and GaN at approximately 3:1, matching the thickness of each layer. This data shows the SL is a good candidate for cladding layers and distributed Bragg reflectors (DBRs) for laser diodes and waveguides to

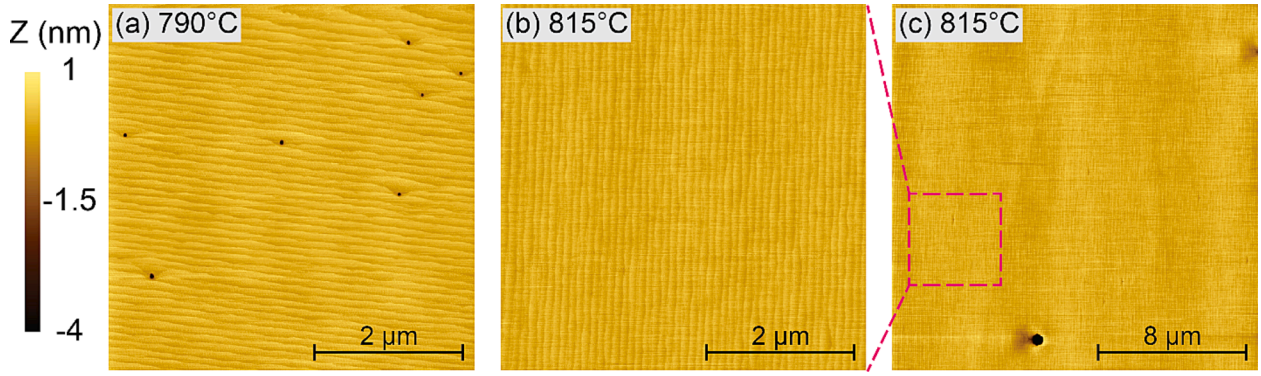


**Fig. 5.** Atomic force microscope (AFM) images of 20-period AlInN/GaN SLs grown on bulk GaN substrates at 30 kPa and (a) 790 °C and (b-c) 815 °C, with In contents of 0.195 and 0.137, respectively. The AFM in (a) shows a smooth surface with clear and parallel GaN atomic steps, with 7 pits on a 5x5 μm AFM scan, with a density of $\sim 1.2 \times 10^7$ cm$^{-2}$. The AFM in (b) shows a better surface with no pits, and a larger 20 x 20 μm scan (c) reveals one pit.

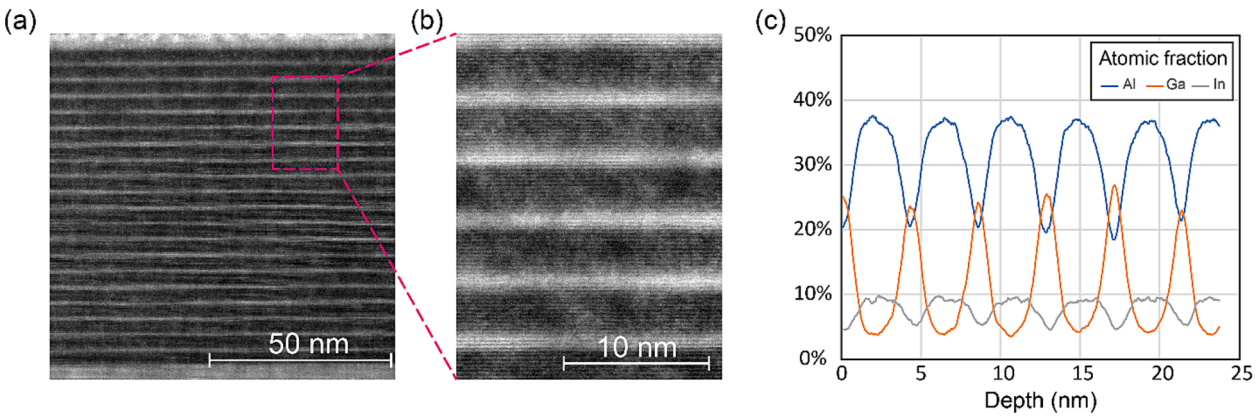


**Fig. 6.** Scanning transmission electron microscope (STEM) images of AlInN/GaN SLs grown on bulk GaN substrate of the full SL (a) and a closeup image (b). Plot of (c) atomic fraction for Al, In, and Ga, versus depth of group III elements in the SL determined by energy-dispersive X-ray spectroscopy (EDS). The STEM and EDS data show a highly periodic layer structure with some level of intermixing between the GaN and AlInN layers.

replace AlGaN. It has the advantage of being lattice matched to GaN and having a lower refractive index (n). For example, the $Al_yGa_{1-y}N$ clad in a laser diode typically has an Al-content of no more than $y = 0.15$. An $Al_{0.15}Ga_{0.85}N$ layer has $n = 2.54$ at 400 nm [39], while the AlInN/GaN shown here is lower at $n = 2.28$ at 400 nm. AlInN has been used in lasers, but the AlInN/GaN SL shown here has better morphology.

Fig. 7 (b) and (c) show the emission from the AlInN/GaN SL grown on a GaN substrate (Fig. 5(b)) using CL. The acceleration voltage is changed to vary the electron penetration depth and identify the emission location. At the lowest voltage of 2 kV, emission with a peak of ~ 317 nm is observed. This light is from the SL and the transitions between electron and hole quantum ground states within the thin GaN layers sandwiched by the wider bandgap AlInN layers. Its energy is 3.91 eV, which is significantly higher than the bandgap of GaN, and is a result of the high band offsets (~1 eV) and thin GaN layers. The wavelength of this emission is consistent with the ground state energy transition simulated using a Schrödinger-Poisson solver. At higher voltages, the intensity of the SL peak grows, and a longer wavelength peak emerges at ~ 365 nm caused by emission from the underlying GaN.

Both the refractive index and emission data show the potential of the AlInN/GaN in photonic devices. The low refractive index and short wavelength emission (or high bandgap absorption) of the SL show it is a candidate for cladding or DBR layers in laser diodes as a replacement for bulk AlInN layers. The SL light emission at wavelengths much shorter than GaN makes it a potential active layer for ultra-violet emitters.

## 4. Conclusion

AlInN/GaN SLs with near-lattice-matched AlInN layers are grown with varying temperatures, pressures, and thicknesses on two types of GaN substrates. The SLs have significantly better surface morphology, avoiding the island growth in bulk AlInN layers. The SL grown on free-standing GaN have nearly perfect step-like surfaces and extremely low pit densities. The SLs have a refractive index that matches the weighted average of the layers, and it emits at 317 nm due to quantum states in the GaN. Growing thicker, higher-quality AlInN/GaN layers could be useful for future optoelectronic and electronic devices.

## CRediT authorship contribution statement

**Haotian Xue:** Conceptualization, Methodology, Software, Validation, Formal analysis, Investigation, Data curation, Writing – original draft, Writing – review & editing, Visualization. **Elia Palmese:** Conceptualization, Methodology, Validation, Formal analysis, Investigation, Data curation, Writing – review & editing, Visualization. **Ben J. Sekely:** Investigation, Resources, Data curation, Writing – review & editing. **Brian D. Little:** Writing – review & editing, Project administration, Investigation, Data curation. **Fred A. Kish:** Writing – review & editing, Project administration, Supervision, Funding acquisition. **John F. Muth:** Resources, Writing – review & editing, Supervision, Funding acquisition. **Jonathan J. Wierer:** Conceptualization, Methodology, Validation, Formal analysis, Investigation, Resources, Writing – original

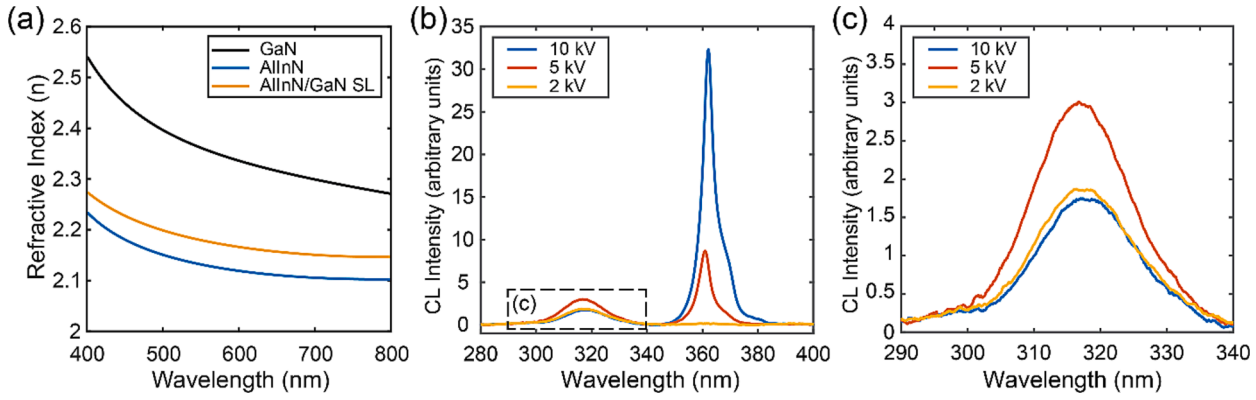


**Fig. 7.** Plot of (a) the refractive index versus wavelength of bulk GaN, AlInN, and an AlInN/GaN SL. Plot of (b) cathodoluminescence (CL) intensity versus wavelength from the SL grown on a GaN substrate at acceleration voltages of 2 kV, 5 kV, and 10 kV. The SL and underlying GaN emit at ~ 317 nm and ~ 365 nm, respectively. The GaN peak dominates at higher voltages where the electrons can penetrate through the SL. Plot of (c) the SL CL intensity at different acceleration voltages.

draft, Writing – review & editing, Supervision, Project administration, Funding acquisition.

## Declaration of competing interest

The authors declare that they have no known competing financial interests or personal relationships that could have appeared to influence the work reported in this paper.

## Data availability

Data will be made available on request.

## Acknowledgments

JJW, HX, and EP acknowledge funding from the U.S. National Science Foundation (Award numbers 1935295 and 2212639). We gratefully thank the Analytical Instrumentation Facility (AIF), Christopher Winkler, and Roberto Garcia at NC State University for their assistance in STEM measurements. We thank TNSC for their support with the MOCVD growth.

## References

[1] S. Yamaguchi, et al., Structural and optical properties of AlInN and AlGaInN on GaN grown by metalorganic vapor phase epitaxy, J. Cryst. Growth 195 (1–4) (1998) 309–313.
[2] J.F. Carlin, et al., Progresses in III-nitride distributed Bragg reflectors and microcavities using AlInN/GaN materials, Physica Status Solidi B-Basic Solid State Physics 242 (11) (2005) 2326–2344.
[3] S. Yoshida *et al.*, "Electron and hole accumulations at GaN/AlInN/GaN interfaces and conductive n-type AlInN/GaN distributed Bragg reflectors," *Japanese Journal of Applied Physics,* vol. 55, no. 5, 2016.
[4] K. Arakawa *et al.*, "450 nm GaInN ridge stripe laser diodes with AlInN/AlGaN multiple cladding layers," *Japanese Journal of Applied Physics,* vol. 58, no. SC, 2019.
[5] C. Gaquiere, et al., "AlInN/GaN a suitable HEMT device for extremely high power high frequency applications," in, IEEE/MTT-S International Microwave Symposium 2007 (2007) 2145–2148.
[6] M.R. Peart, N. Tansu, J.J. Wierer, AlInN for Vertical Power Electronic Devices, IEEE Trans. Electron Devices 65 (10) (2018) 4276–4281.
[7] M.R. Peart, D. Borovac, W. Sun, R.B. Song, N. Tansu, J.J. Wierer, AlInN/GaN diodes for power electronic devices, Appl. Phys Express 13 (9) (2020) 091006.
[8] M.R. Peart, X.L. Wei, D. Borovac, W. Sun, N. Tansu, J.J. Wierer, Thermal Oxidation of AlInN for III-Nitride Electronic and Optoelectronic Devices, Acs Applied Electronic Materials 1 (8) (2019) 1367–1371.
[9] E. Palmese, H. Xue, R. Song, and J. J. Wierer, "Thermal oxidation of lattice mismatched Al1-xInxN films on GaN," *e-Prime - Advances in Electrical Engineering, Electronics and Energy,* vol. 5, 2023.
[10] E. Palmese, M.R. Peart, D. Borovac, R. Song, N. Tansu, J.J. Wierer, Thermal oxidation rates and resulting optical constants of Al0.83In0.17N films grown on GaN, J. Appl. Phys. 129 (12) (2021) 125105.
[11] R.B. Chung, et al., Growth study and impurity characterization of Al In1−N grown by metal organic chemical vapor deposition, J. Cryst. Growth 324 (1) (2011) 163–167.
[12] D. Borovac, W. Sun, R.B. Song, J.J. Wierer, N. Tansu, On the thermal stability of nearly lattice-matched AlInN films grown on GaN via MOVPE, J. Cryst. Growth 533 (2020) 125469.
[13] M. A. Laurent, S. Keller, and U. K. Mishra, "Comprehensive Analysis of Surface Morphology and Growth Mode of AlInGaN Films," *physica status solidi (a),* vol. 216, no. 1, 2018.
[14] M. Miyoshi, M. Yamanaka, T. Egawa, T. Takeuchi, Microstructure variation in thick AlInN films grown on c-plane GaN on sapphire by metalorganic chemical vapor deposition, J. Cryst. Growth 506 (2019) 40–44.
[15] M. Miyoshi, M. Yamanaka, T. Egawa, and T. Takeuchi, "Epitaxial growth and characterization of approximately 300-nm-thick AlInN films nearly lattice-matched toc-plane GaN grown on sapphire," *Applied Physics Express,* vol. 11, no. 5, 2018.
[16] R. Liu *et al.*, "Generation of misfit dislocations by basal-plane slip in InGaN/GaN heterostructures," *Applied Physics Letters,* vol. 89, no. 20, 2006.
[17] D. Holec, Y. C. Zhang, D. V. S. Rao, M. J. Kappers, C. McAleese, and C. J. Humphreys, "Equilibrium critical thickness for misfit dislocations in III-nitrides," *Journal of Applied Physics,* vol. 104, no. 12, 2008.
[18] S. Einfeldt, H. Heinke, V. Kirchner, D. Hommel, Strain relaxation in AlGaN/GaN superlattices grown on GaN, J. Appl. Phys. 89 (4) (2001) 2160–2167.
[19] M. Shiojiri *et al.*, "Structural and compositional analyses of a strained AlGaN/GaN superlattice," *Journal of Applied Physics,* vol. 100, no. 1, 2006.
[20] Y. Y. Zhang and Y. A. Yin, "Performance enhancement of blue light-emitting diodes with a special designed AlGaN/GaN superlattice electron-blocking layer," *Applied Physics Letters,* vol. 99, no. 22, 2011.
[21] P. Kozodoy, et al., Polarization-enhanced Mg doping of AlGaN/GaN superlattices, Appl. Phys. Lett. 75 (16) (1999) 2444–2446.
[22] M.L. Zhang, et al., Growth and characterization of AlGaN/GaN heterostructure using unintentionally doped AlN/GaN superlattices as barrier layer, Superlattice. Microst. 45 (2) (2009) 54–59.
[23] Y. Kawakami, A. Nakajima, X. Q. Shen, G. Piao, M. Shimizu, and H. Okumura, "Improved electrical properties in AlGaN/GaN heterostructures using AlN/GaN superlattice as a quasi-AlGaN barrier," *Applied Physics Letters,* vol. 90, no. 24, 2007.
[24] Y. Kawakami, X.Q. Shen, G. Piao, M. Shimizu, H. Nakanishi, H. Okumura, Improvements of surface morphology and sheet resistance of AlGaN/GaN HEMT structures using quasi AlGaN barrier layers, J. Cryst. Growth 300 (1) (2007) 168–171.
[25] M. Hansen, et al., Effect Of AlGaN/GaN Strained Layer Superlattice Period On InGaN MQW Laser Diodes, MRS Internet J. Nitride Semicond. Res. 5 (S1) (2014) 14–19.
[26] M. Hansen, et al., Effect of AlGaN/GaN strained layer superlattice period on InGaN MQW laser diodes, Physica Status Solidi a-Applied Research 176 (1) (1999) 59–62.
[27] F.A. Ponce, et al., Microstructure and electronic properties of InGaN alloys, Physica Status Solidi B-Basic Research 240 (2) (2003) 273–284.
[28] Y. Kuwahara *et al.*, "GaInN-Based Solar Cells Using Strained-Layer GaInN/GaInN Superlattice Active Layer on a Freestanding GaN Substrate," *Applied Physics Express,* vol. 4, no. 2, 2011.
[29] J. J. Wierer, D. D. Koleske, and S. R. Lee, "Influence of barrier thickness on the performance of InGaN/GaN multiple quantum well solar cells," *Applied Physics Letters,* vol. 100, no. 11, 2012.
[30] W. C. Lai *et al.*, "The CL emission observation of the InGaN/GaN MQWs V shaped pits with different superlattices underlayers," *Physica Status Solidi C - Current Topics in Solid State Physics, Vol 5, No 6,* vol. 5, no. 6, pp. 1639-+, 2008.
[31] C. Haller, J.-F. Carlin, M. Mosca, M.D. Rossell, R. Erni, N. Grandjean, InAlN underlayer for near ultraviolet InGaN based light emitting diodes, Appl. Phys Express 12 (3) (2019) 034002.
[32] E. R. Buß, U. Rossow, H. Bremers, A. Hangleiter, "Lattice-matched AlInN in the initial stage of growth," Appl. Phys. Lett., vol. 104, no. 16, 2014.
[33] J. Han, et al., OMVPE growth and gas-phase reactions of AlGaN for UV emitters, J. Cryst. Growth 195 (1–4) (1998) 291–296.
[34] X.W. Wang, et al., Improving the homogeneity and quality of InGaN/GaN quantum well exhibiting high In content under low TMIn flow and high pressure growth, Appl. Surf. Sci. 548 (2021).
[35] W. Terashima, S.B. Che, Y. Ishitani, A. Yoshikawa, Growth and characterization of AlInN ternary alloys in whole composition range and fabrication of InN/AlInN multiple quantum wells by RF molecular beam epitaxy Jpn J Appl Phys 2 45 20–23 2006 L539 L42.
[36] H.T. Xue, E. Palmese, R.B. Song, M.I. Chowdhury, N.C. Strandwitz, J. Wierer, "Structural and optical characterization of thin AlInN films on c-plane GaN substrates," J. Appl. Phys., vol. 134, no. 7, 2023.
[37] J.J. Wierer, A.A. Allerman, Q. Li, Silicon impurity-induced layer disordering of AlGaN/AlN superlattices, Appl. Phys. Lett. 97 (5) (2010) 051907.
[38] J. Kim, et al., Origins of unintentional incorporation of gallium in InAlN layers during epitaxial growth, part II: Effects of underlying layers and growth chamber conditions, J. Cryst. Growth 388 (2014) 143–149.
[39] J.F. Muth, et al., Absorption coefficient and refractive index of GaN, AlN and AlGaN alloys, MRS Internet J. Nitride Semicond. Res. 4 (S1) (1999) 502–507.